12-1-2018

Oxygen-induced leakage of spin polarization in Overhauser-enhanced magnetic resonance imaging: Application for oximetry in tumors

Artem A. Gorodetskii
West Virginia University

Timothy D. Eubank
West Virginia University

Benoit Driesschaert
West Virginia University

Martin Poncelet
West Virginia University

Emily Ellis
West Virginia University

See next page for additional authors

HHS Public Access

Author manuscript

J Magn Reson. Author manuscript; available in PMC 2019 December 01.

Published in final edited form as:

J Magn Reson. 2018 December ; 297: 42–50. doi:10.1016/j.jmr.2018.10.005.

Oxygen-induced leakage of spin polarization in Overhauser-enhanced magnetic resonance imaging: application for oximetry in tumors

Artem A. Gorodetskii[a,b,c,d], **Timothy D. Eubank**[a,e], **Benoit Driesschaert**[a,f], **Martin Poncelet**[a,b], **Emily Ellis**[e], **Valery V. Khramtsov**[a,b,*], and **Andrey A. Bobko**[a,b,*]

[a]In Vivo Multifunctional Magnetic Resonance center, Robert C. Byrd Health Sciences Center, West Virginia University, Morgantown, WV 26506, USA

[b]Department of Biochemistry, West Virginia University School of Medicine, Morgantown, WV 26506, USA

[c]N.N. Voroztsov Novosibirsk Institute of Organic Chemistry SB RAS, Novosibirsk, 630090, Russia

[d]Novosibirsk State University, Novosibirsk, 630090, Russia

[e]Department of Microbiology, Immunology & Cell Biology, West Virginia University School of Medicine, Morgantown, WV 26506, USA

[f]Department of Pharmaceutical Sciences, West Virginia University, School of Pharmacy, Morgantown, WV 26506, USA

Abstract

Overhauser-enhanced Magnetic Resonance Imaging (OMRI) is a double resonance technique applied for oxygen imaging in aqueous samples and biological tissues. In this report, we present an improved OMRI approach of oxygen measurement using the single line “Finland” trityl spin probe. Compared to a traditional approach, we introduced an additional mechanism of leakage of spin polarization due to an interaction of a spin system with oxygen. The experimental comparison of the new approach with an oxygen-dependent leakage factor to a traditional approach performed in phantom samples *in vitro*, and mouse tumor model *in vivo*, shows improved accuracy of determination of oxygen and contrast agent concentrations.

Graphical Abstract

Overhauser-enhanced Magnetic Resonance Imaging is used for oxygen imaging in vivo Overhauser signal enhancement depends on contrast agent and oxygen concentrations Overhauser signal enhancement increased with a higher contrast agent concentration The presence of a paramagnetic compounds decreases an Overhauser signal enhancement Polarization leakage factor is important for correct oxygen values assessment

*Corresponding authors valery.khramtsov@hsc.wvu.edu; andrey.bobko@hsc.wvu.edu.

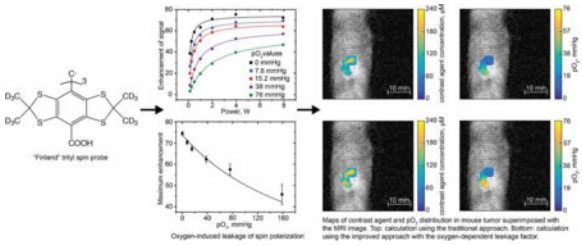

Keywords

Overhauser-enhanced magnetic resonance imaging (OMRI); proton-electron double-resonance imaging (PEDRI); leakage of spin polarization; trityl radical; oximetry; tumor tissue oximetry

Introduction

Oxygen level in living tissues is a key parameter that can contribute to progression of solid tumor. Rapid tumor growth results in insufficient tumor vascularization accompanied by significant changes in the tissue microenvironment such as hypoxia [1]. Hypoxia is a main prognostic factor in tumor treatment [2], therefore noninvasive quantitative measurement of oxygen concentration in tissues provides a solid basis to distinguish between normal and tumor tissues and to study hypoxia mechanisms and dynamics.

Magnetic resonance techniques are important noninvasive oximetric methods in in vivo studies. Various NMR-based methods are utilized for oxygen imaging *in vivo*. Blood oxygen level-dependent (BOLD) MRI is widely used for studying brain and tumor oxygenation. However, this approach does not provide direct oxygen concentration measurements, therefore statistical analysis must be used to recalculate BOLD MRI data to pO_2 values [3, 4]. Fluorocarbon contrast agent-based ^{19}F MRI is a recently developed approach for quantitative oxygen imaging [5, 6]. Electron paramagnetic resonance (EPR) - based approaches with use of specially designed paramagnetic spin probes also allow for direct pO_2 determination with high resolution but suffer a lack of anatomical information [7–9]. The combination of ^{1}H MRI and EPR imaging (EPRI) techniques allows for co-registration of both anatomical and functional information and are, therefore excellent tools for visualization of oxygen concentration with high spatial and temporal resolution [10–12]. Overhauser-enhanced magnetic resonance imaging (OMRI, also termed proton-electron double-resonance imaging, PEDRI) is a unique double resonance imaging technique that allows for simultaneous mapping of functional and anatomical information [13]. Exogenous paramagnetic probes are used in OMRI similar to standard EPRI approaches. OMRI is based on the Overhauser effect, which is the transfer of electron spin polarization (created by applying the EPR irradiation at spin probe resonance frequency) to protons of water [14]. Polarization transfer results in enhancement of MRI signal intensity. The degree of enhancement depends on several factors: EPR irradiation power, rates of cross-relaxation processes, protons relaxation time, and electron spin relaxation times of the contrast agent. Molecular oxygen is paramagnetic which enables interaction with both with a spin probe and protons resulting in decreased enhancement of an MRI signal. Therefore providing an opportunity for direct quantitative measurement of oxygen [15].

OMRI has been used for imaging oxygen in aqueous samples and biological tissues *in vivo* [13, 15–17]. It has been found that acquisition of two MRI images at two different EPR irradiation powers and one MRI image with EPR-off irradiation is required to visualize both oxygen and contrast agent concentrations.

In previous works [15–18] the influence of oxygen concentration on MRI signal enhancement has been analyzed considering an exclusive oxygen effect on spin probe relaxation times. Therefore, at a high power limit (when saturation factor is equal to 1) signal enhancement depends only on the concentration of contrast agent. However, in our current work, we demonstrate that MRI signal enhancement at high irradiation powers also depends on oxygen concentration in solution. Accordingly, the equation previously used to describe the behavior of signal enhancements [15–18] has to be modified to accommodate additional mechanisms of oxygen influence. Of note, the mechanism of influence of an additional paramagnetic agent on the Overhauser effect in the system of two spins is well known, and a corresponding factor can be introduced as leakage relaxation rate into the Solomon equations [19–21].

In this report, we developed an improved OMRI approach to measure oxygen concentration. We introduce a new definition of a leakage factor, which contains a dependence on oxygen concentration. This improvement leads to enhanced accuracy of oxygen and contrast agent concentrations measurement.

Materials and Methods

3.1 Chemicals

Deuterated “Finland” trityl radical (Figure 1) used as a paramagnetic oxygen-sensitive agent was synthesized according to published procedure [22]. Nitroxide radical 3-carbamoyl-PROXYL and contrast agent Gd-DTPA were purchased from the Sigma–Aldrich and BioPal, respectively.

3.2 OMRI scanner, pulse sequence and experimental parameters

The OMRI experiments were performed on an OMRI desk top imager (Keller JXI-KC02, Japan Redox Ltd.) using a standard fast spin echo sequence for MRI. The imager is equipped with permanent magnet producing B_0 field of 16 mT. The EPR irradiation was applied for 500 ms (T_{EPR}) at a frequency of 451.9 MHz. This frequency corresponds to the maximum value of spin probe dynamic nuclear polarization spectrum. Scan parameters T_R and T_E were 700 ms and 37 ms for 2D and 1200 ms and 37 ms for 3D mode, echo factor was 4. Field of view was 30×30 mm^2 for phantom imaging and 40×40 mm^2 for animal imaging, matrix size was 64×64 for 2D, and 32×32 for 3D modalities. Slice thickness was 100 mm for phantom samples and 4 mm for experiments with animals. Number of averages was 10 for MRI (EPR-off) images, 2 for 2D and 1 for 3D OMRI images. Acquisition times for one image were 13 s and 80 s for 2D and 3D modalities, respectively.

3.3 Theory

The Overhauser enhancement, E, for the system of two spins ½, where S is an electron spin of a contrast agent and I is a spin of water proton, is described by equation [14]:

$$E = \left|I_z/I_0\right| = \left|1 - \left(\gamma_S/\gamma_I\right) \cdot \varepsilon \cdot f \cdot S\right|, \quad (1)$$

where I_Z and I_0 are nuclear spin polarizations in the presence and absence of EPR irradiation, correspondingly; γ_S and γ_I are the values of gyromagnetic ratio of electron and proton, correspondingly; ε is a coupling factor that characterizes an efficacy of coupling (polarization transfer) between nuclear and electron spins; f is a leakage factor that characterizes efficacy of proton relaxation in the presence of the contrast agent; S is a saturation factor that determines saturation degree of electron energy level.

The spin states diagram for the radical contrast agent with an electron spin of ½ and a solvent proton spin of ½ has four energy levels connected by the transitions as shown in Figure 2. The leakage factor can be determined via the rates of these transitions and written as a function of radical concentration:

$$f(C) = \frac{2w_I + w_0 + w_2}{2w_I + w_0 + w_2 + w^0} = 1 - T_1/T_{10} = \frac{r \cdot C \cdot T_{10}}{1 + r \cdot C \cdot T_{10}}, \quad (2)$$

Where w^0 and w_I are the ^{1}H transition rates in the absence and presence of the radical; w_0 and w_2 - are the rates of zero and double quantum transitions induced by dipole-dipole and contact interactions; T_1 and T_{10} are the relaxation times of water protons in the presence and absence of spin probe, correspondingly; r– is the relaxivity; C– is the concentration of the radical.

The saturation factor is a function of applied irradiation power [14]:

$$S\left(P, C, C_{O_2}\right) = \frac{\alpha \cdot P}{1/\left(\gamma_S^2 T_{1e} T_{2e}\right) + \alpha \cdot P}, \quad (3)$$

where α is a resonator efficiency factor experimentally measured for each sample in separate experiment, T_{1e} and T_{2e} are contrast agent electron spin relaxation times. The influence of contrast agent and oxygen concentrations on relaxation times can be expressed by the following equation [15]:

$$1/\left(\gamma_S^2 T_{1e} T_{2e}\right) = \left(a_0 + a_1 \cdot C + a_2 \cdot C_{O_2}\right)^2, \quad (4)$$

where a_0, a_1, and a_2 are experimentally calibrated parameters.

An enhancement of MRI signal can be expressed as a function of irradiation power, and concentrations of the contrast agent and oxygen:

$$E = \left|1 - \left(\gamma_S/\gamma_I\right) \cdot \varepsilon \cdot f(C) \cdot S\left(P, C, C_{O_2}\right)\right|. \quad (5)$$

The maximum enhancement at infinite power can be expressed as follows:

$$E_{max} = E(P \to \infty) = \left|1 - \left(\gamma_S/\gamma_I\right) \cdot \varepsilon \cdot f(C)\right|. \quad (6)$$

In this formalism, the maximum enhancement does not depend on oxygen concentration which is in contradiction with the experimental data (see Figure 4B). Therefore, we suggested considering an additional mechanism of leakage of spin polarization due to interaction of spin system with oxygen [19, 20]. Oxygen is a paramagnetic molecule and its interaction with spin system should contribute into decay of spin polarization at any irradiation power. Therefore, we introduce an additional relaxation rate, w_l, proportional to oxygen concentration in the leakage factor:

$$w_l = w_l^0 \cdot C_{O_2}, \quad (7)$$

$$f^*\left(C, C_{O_2}\right) = \frac{2w_I + w_0 + w_2}{2w_I + w_0 + w_2 + w^0 + w_l} = f(C) \cdot f_{oxy}\left(C, C_{O_2}\right),$$

$$f_{oxy}\left(C, C_{O_2}\right) = \frac{1}{1 + T_1 \cdot w_l} = \frac{1}{1 + w_l^0 \cdot C_{O_2} \cdot T_{10}/\left(1 + r \cdot C \cdot T_{10}\right)},$$

Where w_l^0 is a leakage rate constant; C_{O_2} is the oxygen concentration; $f(C)$ is the leakage factor as described previously in equation (2). Therefore, enhancement of MRI signal is determined as:

$$E = \left|1 - \left(\gamma_S/\gamma_I\right) \cdot \varepsilon \cdot f^*\left(C, C_{O_2}\right) \cdot S^*\left(P, C, C_{O_2}\right)\right|. \quad (8)$$

The maximum enhancement at infinite power in this formalism does depend on oxygen concentration and can be expressed as follows:

$$E_{max} = \left|1 - (\gamma_S/\gamma_I) \cdot \varepsilon \cdot f^*\left(C, C_{O_2}\right)\right| = \left|1 - (\gamma_S/\gamma_I) \cdot \varepsilon \cdot \frac{r \cdot C \cdot T_{10}}{1 + r \cdot C \cdot T_{10}} \cdot \frac{1}{1 + T_1 \cdot w_l^0 \cdot C_{O_2}}\right| \quad (9)$$

3.4 Data processing and oxygen calculation procedure

An enhancement of MRI signal depends on both spin probe and oxygen concentration, therefore measurement of enhancements at two different powers is sufficient to solve the following system of two equations:

$$E_1 = \left|1 - (\gamma_S/\gamma_I) \cdot \varepsilon \cdot f(C) \cdot S\left(P_1, C, C_{O_2}\right)\right|, \quad (10)$$

$$E_2 = \left|1 - (\gamma_S/\gamma_I) \cdot \varepsilon \cdot f(C) \cdot S\left(P_2, C, C_{O_2}\right)\right|.$$

Note that acquisition of a third MRI image with no EPR irradiation power is required to calculate the enhancement value. A similar system of two equation might be written for the case of a new definition of leakage factor *f**, namely:

$$E_1 = \left|1 - (\gamma_S/\gamma_I) \cdot \varepsilon \cdot f^*\left(C, C_{O_2}\right) \cdot S^*\left(P_1, C, C_{O_2}\right)\right|, \quad (11)$$

$$E_2 = \left|1 - (\gamma_S/\gamma_I) \cdot \varepsilon \cdot f^*\left(C, C_{O_2}\right) \cdot S^*\left(P_2, C, C_{O_2}\right)\right|.$$

In order to calculate oxygen and contrast agent concentrations systems of equations (10) and (11) were solved numerically. For this purpose all unknown parameters of the model had been obtained in calibration experiments (coupling factor ε relaxation time of water protons, T_{10}; relaxivity, r; leakage rate constant, w_l^0; parameters a_0, a_1, a_2). All data processing procedures were made using specially developed MATLAB code.

Parameters T_{10} and r were found by the saturation recovery experiment with samples with different contrast agent concentrations (0, 0.5, 1, 2 mM) in anaerobic conditions. We have found that values of T_{10} = 3.9±0.1 s and r = 0.12±0.01 $(\text{mM}\cdot\text{s})^{-1}$ in good agreement with published data [23, 24].

The coupling factor ε was obtained using the following procedure. The dependence of the Overhauser enhancement on microwave power was obtained at different concentrations of the spin probe in anaerobic conditions (see Figure 3A) and the data were fitted using the following equation to extract the maximum enhancement value, E_{max} [25]:

$$E = -1 + A \cdot P/(1 + B \cdot P), \quad (12)$$

$$E_{max} = -1 + A/B.$$

The dependence of E_{max} on the contrast agent concentration (see Figure 3B) was approximated by equation (9) yielding a value of the coupling factor ε equal to 0.357±0.003 in agreement with published value [23].

Parameters, a_0, a_1, a_2 and w_l^0 were found using a global fitting procedure. A set of experimental data of measured enhancements at different irradiation powers, contrast agent and oxygen concentrations was analyzed using equations (5) or (8) where parameters a_0, a_1, a_2 and w_l^0 were global fitting parameters. Parameters a_0, a_1, a_2 were equal to 0.45±0.03 μT, 0.42±0.01 μT/mM, (48±1)×10^{-3} μT/mmHg for calculations with factor f and 0.48±0.02 μT, 0.41±0.01 μT/mM, (34±1)×10^{-3} μT/mmHg for calculations with factor f^*. Leakage rate constant w_l^0 was equal to (1.7±0.2)×10^{-3} (mmHg·s)$^{-1}$. These parameters were used for all following calculations.

The resonator efficiency factor α was measured for each sample using Time Domain Sensor (SPEAG) as proportional coefficient between square of magnetic field B_1 and EPR irradiation power.

3.5 Phantom samples preparation and imaging

The contrast agent was dissolved in 150 mM NaCl solution for samples preparation. Sample solutions were bubbled during 15 minutes with gas mixture of nitrogen and oxygen in various proportions to provide desired oxygen concentration. All measurements were performed at 33 °C. All calibration samples consisted of one 8 ml tube filled with 5 ml of contrast agent solution and one 8 ml tube filled with 150 mM NaCl solution. The resonator efficiency factor α for the calibration experiments was 6.1 μT^2/W. Set of dependences of enhancement of MRI signal on irradiation power at contract agent concentrations 0.25, 0.5, 1, 2, 4 mM and oxygen partial pressures 0, 7.6, 15.2, 38, 76 and 159 mmHg were obtained. OMRI data were acquired at irradiation powers 0, 0.125, 0.25, 0.5,1, 2, 4 and 8 W for all calibration experiments and mean data values of OMRI images from regions of interest for each sample were used for further data processing.

The phantom sample consisted of four 2 ml tubes filled with 0.25, 0.5, 1, 2 mM contrast agent solution at oxygen partial pressures 0, 15.2, 38 and 76 mmHg. One 2D MRI and two 2D OMRI images were acquired at irradiation powers 0, 0.5 and 8.0 W. In order to map oxygen and contrast agent concentration system of equations (10 or 11) was solved numerically in each pixel of images set as described above.

3.6 Animals imaging *in vivo*

All animal work was performed in accordance with the WVU IACUC approved protocol.

MMTV-PyMT (polyoma virus middle T antigen) transgenic mice which spontaneously-develop breast cancer were used for *in vivo* experiments. A stock solution of 15 mM contrast agent (pH=7.1) in 150 mM sodium chloride solution was prepared for injection in mouse tumors. Injection solution was bubbled slowly during 30 minutes with gas mixture of nitrogen and oxygen in proportion 93%/7% to provide faster equilibration of tumor microenvironment after injection. Animal was placed into OMRI resonator and anesthetized by inhalation of air-isoflurane mixture using DRE VP3 (DRE veterinary, USA) anesthetic machine. Tube with gas mixture was connected to back side of resonator to provide continuous gas supply during experiment. After onset of anesthesia resonator efficiency factor was measured and 70 μl of stock solution of contrast agent was injected into mouse tumor for 2D experiment and 300 μl of stock solution for 3D experiment. Fifteen minutes after injection one MRI and two OMRI images were acquired at irradiation powers 0, 1 and 8 W for 2D modality and 0, 1 and 16 W for 3D modality. The observed values of enhancements ranged from 5 to 20 for high power (8 W) and from to 2 to 14 for low power (1 W) in the 2D experiment. The corresponding enhancements ranged from 2 to 14 for high power (16 W) and from 1 to 4 for low power (1 W) in the 3D experiment. Slice thickness of 4 mm was selected for 2D modality so that only signals from area with contrast agent contributed to the enhancement. In order to map oxygen and contrast agent concentration the system of equations was solved numerically in each pixel of image set as described above. For computation in the tumors the same values of the parameters, T_{10}, r, ε, a_0, a_1, a_2, and w_l^0 were used as for the phantom samples.

Results and Discussion

4.1 Leakage of spin polarization

Signal enhancement in the OMRI experiments strongly depends on EPR irradiation power and contrast agent concentration as illustrated in Figure 3A. As expected, signal enhancement increases with concentration (leakage factor, f) and power (saturation factor, S) increase. Fitting equation (12) to experimental data allows for extraction of maximum enhancement value E_{max} at various contrast agent concentrations shown in Figure 3B. Fitting dependence of E_{max} on contrast agent concentration (see Figure 3B) using equation (6) yields values of coupling factor ($\varepsilon = 0.357 \pm 0.003$) and enhancement at infinitive power and contrast agent concentration $\left(E_{max}^{inf} = 236 \pm 2\right)$ that agree with previously published data [15, 23].

Paramagnetic oxygen molecule interacts both with spin probe and water protons which may result in alteration of OMRI enhancement. Figure 4A shows a dependences of enhancement on irradiation power for samples with contrast agent concentration of 1 mM and different oxygen concentrations. In agreement with Figure 3, the enhancement value is growing with increasing EPR power. Fitting the data to equation (12) yields the values of E_{max} shown in Figure 4B that demonstrates E_{max} decrease with increasing oxygen concentration.

Paramagnetic molecules interact with water resulting in shortened longitudinal relaxation time of protons. Therefore, an enhancement of OMRI signal in the solution of contrast agent is decreased in the presence of paramagnetic species such as oxygen (see [26]). Equation (9) allows us to correctly describe the dependence of E_{max} on oxygen concentration at high powers when saturation factor value is close to 1 (Figure 4B). Fitting the dependence of E_{max} on oxygen partial pressures using equation (9) yields the value of leakage rate constant, w_l^0, equal to 1.3±0.2 $(\text{mM}\cdot\text{s})^{-1}$ ($w_l^0 = (1.7 \pm 0.2) \times 10^{-3} (\text{ mmHg}\cdot\text{s})^{-1}$, assuming solubility of oxygen 1.0 mM at 1 atm [27]).

To test whether the presence of any additional paramagnetic molecules in the spin probe solution will result in leakage of polarization, we performed measurements of trityl radical-induced OMRI enhancement in the presence of the nitroxide radical, 3-carbamoyl-PROXYL, and gadolinium complex, Gd-DTPA (see Figure 5A and5B). Leakage rate constants were found to be equal to 0.11±0.02 and 5.0±0.3 $(\text{mM}\cdot\text{s})^{-1}$ for the nitroxide and gadolinium complex, respectively.

Effective proton relaxation time in the presence of OMRI-active contrast agent and additional paramagnetic agent can be described as following:

$$\frac{1}{T_{10}^{eff}} = \frac{1}{T_{10}^{0}} + r_{par} \cdot C_{par}, \quad (13)$$

where T_{10}^0 – water relaxation time in the absence of paramagnetic compound, r_{par} and C_{par} – relaxivity and concentration of paramagnetic compound, respectively. Therefore, leakage rate $w_l = w_l^0 \cdot C_{par} = r_{par} \cdot C_{par}$. Experimental data (saturation recovery experiment for different oxygen and Gd concentration was performed to measure corresponding relaxivities) for oxygen relaxivity in PBS solution show the value of $(4.5\pm0.2)\times10^{-4}$ $(\text{mmHg}\cdot\text{s})^{-1}$ compare to literature data 5.0 to 6.6×10^{-4} $(\text{mmHg}\cdot\text{s})^{-1}$ [28]. Note that relaxivity of oxygen is two-three times smaller than leakage rate constant obtained in the OMRI experiment. Contradictory to oxygen experiments, relaxivity of gadolinium was found to be 6.7±0.3 $(\text{mM}\cdot\text{s})^{-1}$ (literature data 6.5–7.0 $(\text{mM}\cdot\text{s})^{-1}$ [29, 30]) which is comparable to the leakage rate constant w_l^0 obtained in the OMRI experiments. Similar to the Gd-DTPA, the reported relaxivity of the nitroxide radical, 0.4 $(\text{mM}\cdot\text{s})^{-1}$ [31] is several fold larger than the leakage rate constant w_l^0 measured in OMRI experiments.

It is no surprise that the value of relaxivity for both gadolinium and nitroxide radical is higher than the leakage rate constant w_l^0 because of (i) partial overlap of the dynamic nuclear polarization spectra of paramagnetic compounds for the OMRI experiment with “Finland” contrast agent in the presence of nitroxide; and (ii) influence of Heisenberg exchange with paramagnetic compounds, especially for the case of the nitroxide radical. However, significantly lower relaxivity value r compare to leakage rate constant w_l^0 is phenomena

which could not be explained and has to be investigated both experimentally and theoretically.

Experimental data shown in Figure 4A can be satisfactorily fitted by both equations (5) and (8). The values of contrast agent and oxygen concentrations as prepared for the samples and obtained from the fittings are listed in Table 1. As it has been noted, plateau value of enhancement and corresponding E_{max} values decrease upon increase of oxygen partial pressure (see Figure 4). Consequently, use of equation (5) results in a decrease of calculated values of the contrast agent concentration (see Table 1) upon increase of oxygen to compensate for the absence of oxygen effect on E_{max}. In case of equation (8), a "plateau" level of enhancement is governed by oxygen-dependent leakage factor and calculated values of contrast agent and oxygen concentrations are in satisfactory agreement with those prepared.

4.2 Phantom imaging

In order to compare the accuracy of both methods of calculations, we performed OMRI acquisition of phantom samples to generate 2D maps of oxygen and contrast agent concentrations. Using a minimal number of image acquisitions only at two different powers is justified by its relevance to *in vivo* studies when experimental time of functional mapping of living tissue is limited. Maps of contrast agent and pO_2 distribution were calculated using two different models with leakage factors f and f^* are shown in Figure 6. The corresponding values of contrast agent and pO_2 as prepared for the phantom samples and the mean values obtained from the fittings are listed in the Table 2.

It is clear that the mean values obtained with the factor f^* are in satisfactory agreement with the prepared values while use of the factor results in underestimation of both pO_2 and contrast agent concentration, especially at their high values.

4.3 Animal imaging

Figure 7 shows pO_2 and contrast agent concentrations 2D maps obtained by OMRI in mouse tumor (5×8 mm, caliper measurement). System of equations was solved in each pixel using set of images and solutions were obtained using two calculation models with leakage factors f and f^*. Values of enhancements varied in the range from 5 to 20 for high power and from 2 to 14 for low power. Functional maps were superimposed with MRI image. Oxygen maps show two clearly distinguished regions of hypoxic and normoxic tissue microenvironments. Mean oxygen partial pressure and its standard deviation were found to be equal to 17±7 mmHg and 23±9 mmHg in hypoxic region when calculated with the leakage factors f and f^*, correspondingly. The oxygen partial pressures for normoxic tissues are 2–3 fold higher and equal to 43±5 mmHg (calculated with factor f) and 60±8 mmHg (calculated with factor f^*). Mean oxygen partial pressures for the whole tumor were found to be equal to 24 mmHg and 34 mmHg for calculations with leakage factors f and, f^* correspondingly. Of note, lower spin probe concentrations were calculated in the normoxic tissue using the model with factor f compared with the value calculated using factor f^* It can be suggested that the decreased values of the spin probe and oxygen partial pressures calculated in the model with factor f is

a consequence of the correction of enhancement asymptotic at high powers as has been shown on phantom samples.

Figure 8 (A-H) shows pO_2 and contrast agent concentrations 3D maps in mouse tumor (15×25 mm, caliper measurement), their 2D projection in the coronal plane and distribution of pO_2 values calculated from 3D maps. The mean values and standard deviations calculated for the models with factors f and f^* are equal to 27±7 mmHg and 38±9 mmHg, correspondingly. Measured pO_2 values were found to be in agreement with values measured by L-band EPR spectroscopy[32].

4.4 Calculation parameters: choice of water proton relaxation time

Calculations of pO_2 and contrast agent concentration in the tumor was performed using the same value of T_{10} relaxation time as for the phantom samples (T_{10} = 3.9 s). It has been reported that the values of proton relaxation time T_{10} in tumor tissue vary in wide range from 0.2 s to 1.6 s due to the highly heterogeneous tissue properties [26]. Nevertheless, Figure 8I shows that calculated pO_2 values are not significantly affected by variation of T_{10} value in the range of 1–4 s. The further decrease in value from 1 s to 0.2 s significantly affects calculated values of pO_2 (Fig. 8I). However this decrease in T_{10} is accompanied by increasing of the relaxivity of trityl probes [23]. Figures 8K shows the dependence of mean pO_2 value on relaxivity value at T_{10} = 0.2 s (blood) and 0.5 s (plasma) [33]. An increase of relaxivity value results in increase of calculated pO_2, therefore, compensating the effects of low value of T_{10} (Figures 8I and 8K). These compensatory effects of proton T_{10} and trityl relaxivity changes on the value of calculated pO_2 can be illustrated for “Finland” trityl radical. The relaxivity of this probe was measured to be equal to 0.15 (water, saline), 0.5 (plasma) and 0.6 (whole blood) $M^{-1}s^{-1}$ [23] and the corresponding T_{10} values were reported to be equal to 3.9 s (measured in this paper), 0.5 s and 0.2 s [33]. The corresponding calculations yield similar mean values of pO_2 (± standard deviations) equal to 38±9 mmHg for T_{10} = 3.9 s and r = 0.12 $M^{-1}s^{-1}$, 37±9 mmHg for T_{10} = 0.5 s and r = 0.5 $M^{-1}s^{-1}$, and 35±8 mmHg for T_{10} = 0.2 s and r = 0.6 $M^{-1}s^{-1}$. In these cases changing of T_{10} and r is completely compensated by increasing of calculated spin probe concentration (Figures 8J and 8L). Therefore, the discussed “compensatory effect” justifies the use of uniform saline–based set of T_{10} and relaxivity parameters for *in vivo* data calculation of heterogeneous tissues.

Finally, we can conclude that neglecting an influence of oxygen on maximum signal enhancement leads to calculation error approximately 10 mmHg for normally oxygenated areas. This error is caused by abnormal behavior of the model at high EPR pumping powers.

Conclusion

In summary, an improved approach for oxygen concentration calculations using the OMRI technique has been presented. Our proposed improvement corrects the dependence of MRI signal enhancement at high powers in the presence of oxygen that results in an increase of the accuracy of the measurements of oxygen and contrast agent concentrations. A new approach has been used for 2D and 3D oxygen mapping in mouse tumors and phantom samples. It has been demonstrated that neglecting oxygen influence on maximum signal

enhancement at high oxygen partial pressures in the range from 30 mmHg to 80 mmHg can lead to calculation error in oxygen partial pressures up to 10–20 mmHg.

Acknowledgements

This work was partially supported by NIH grants CA194013, CA192064, U54GM104942, EB023990 and P20GM121322. The content is solely the responsibility of the authors and does not necessarily represent the official views of the NIH. The WVCTSI is acknowledged for start-up to VVK, AAB, and TDE. The authors thank Prof. E. G. Bagryanskaya for the useful discussion. A. A. Gorodetskii thanks by the Ministry of Education and Science of the Russian Federation (state contract no. 2017–220-06–7355) for financial support.

References

[1]. Pacheco-Torres J, Lopez-Larrubia P, Ballesteros P, Cerdan S, Imaging tumor hypoxia by magnetic resonance methods, NMR Biomed, 24 (2011) 1–16. [PubMed: 21259366]

[2]. Brizel DM, Sibley GS, Prosnitz LR, Scher RL, Dewhirst MW, Tumor hypoxia adversely affects the prognosis of carcinoma of the head and neck, Int J Radiat Oncol Biol Phys, 38 (1997) 285–289. [PubMed: 9226314]

[3]. Zhang JL, Morrell G, Rusinek H, Warner L, Vivier PH, Cheung AK, Lerman LO, Lee VS, Measurement of renal tissue oxygenation with blood oxygen level-dependent MRI and oxygen transit modeling, Am J Physiol Renal Physiol, 306 (2014) F579–587. [PubMed: 24452640]

[4]. Thacker J, Zhang JL, Franklin T, Prasad P, BOLD quantified renal pO2 is sensitive to pharmacological challenges in rats, Magn Reson Med, 78 (2017) 297–302. [PubMed: 27501515]

[5]. Zhao D, Jiang L, Hahn EW, Mason RP, Comparison of 1H blood oxygen level-dependent (BOLD) and 19F MRI to investigate tumor oxygenation, Magn Reson Med, 62 (2009) 357–364. [PubMed: 19526495]

[6]. Hallac RR, Zhou H, Pidikiti R, Song K, Stojadinovic S, Zhao D, Solberg T, Peschke P, Mason RP, Correlations of noninvasive BOLD and TOLD MRI with pO2 and relevance to tumor radiation response, Magn Reson Med, 71 (2014) 1863–1873. [PubMed: 23813468]

[7]. Epel B, Halpern HJ, In Vivo pO2 Imaging of Tumors: Oxymetry with Very Low-Frequency Electron Paramagnetic Resonance, Methods Enzymol, 564 (2015) 501–527. [PubMed: 26477263]

[8]. Hyodo F, Matsumoto S, Devasahayam N, Dharmaraj C, Subramanian S, Mitchell JB, Krishna MC, Pulsed EPR imaging of nitroxides in mice, J Magn Reson, 197 (2009) 181–185. [PubMed: 19157932]

[9]. Khramtsov VV, In vivo molecular EPR-based spectroscopy and imaging of tumor microenvironment and redox using functional paramagnetic probes, Antioxid Redox Signal, 28 (2018) 1365–1377. [PubMed: 29132215]

[10]. Ohfuchi M, Goodwin J, Fujii H, Hirata H, Three-Dimensional EPR/NMR Image Coregistration Using a MATLAB-Based Software, Concept Magn Reson B, 39b (2011) 180–190.

[11]. Subramanian S, Krishna MC, Electron paramagnetic resonance imaging, Resonance, 21 (2016) 717–740.

[12]. Ahmad R, Caia G, Potter LC, Petryakov S, Kuppusamy P, Zweier JL, In vivo multisite oximetry using EPR-NMR coimaging, J Magn Reson, 207 (2010) 69–77. [PubMed: 20850361]

[13]. Kishimoto S, Krishna MC, Khramtsov VV, Utsumi H, Lurie DJ, In vivo application of proton electron double resonance imaging, Antioxid Redox Signal, 28 (2018) 1345–1364. [PubMed: 28990406]

[14]. Hausser KH, Stehlik D, Dynamic nuclear polarization in liquids, in: Advances in Magnetic and Optical Resonance, Elsevier, 1968, pp. 79–139.

[15]. Golman K, Petersson JS, Ardenkjaer-Larsen JH, Leunbach I, Wistrand LG, Ehnholm G, Liu K, Dynamic in vivo oxymetry using overhauser enhanced MR imaging, J Magn Reson Imaging, 12 (2000) 929–938. [PubMed: 11105032]

[16]. Krishna MC, English S, Yamada K, Yoo J, Murugesan R, Devasahayam N, Cook JA, Golman K, Ardenkjaer-Larsen JH, Subramanian S, Mitchell JB, Overhauser enhanced magnetic resonance

imaging for tumor oximetry: coregistration of tumor anatomy and tissue oxygen concentration, Proc Natl Acad Sci U S A, 99 (2002) 2216–2221. [PubMed: 11854518]

[17]. Matsumoto S, Yasui H, Batra S, Kinoshita Y, Bernardo M, Munasinghe JP, Utsumi H, Choudhuri R, Devasahayam N, Subramanian S, Mitchell JB, Krishna MC, Simultaneous imaging of tumor oxygenation and microvascular permeability using Overhauser enhanced MRI, Proc Natl Acad Sci U S A, 106 (2009) 17898–17903. [PubMed: 19815528]

[18]. Efimova OV, Caia GL, Sun Z, Petryakov S, Kesselring E, Samouilov A, Zweier JL, Standard-based method for proton-electron double resonance imaging of oxygen, J Magn Reson, 212 (2011) 197–203. [PubMed: 21807539]

[19]. Borgias BA, James TL, Two-dimensional nuclear Overhauser effect: complete relaxation matrix analysis, Methods Enzymol, 176 (1989) 169–183. [PubMed: 2811685]

[20]. Macura S, Ernst RR, Elucidation of cross relaxation in liquids by two-dimensional N.M.R. spectroscopy (Reprinted from Molecular Physics, vol 41, pg 95–117, 1980), Mol Phys, 100 (2002) 135–147.

[21]. Solomon I, Relaxation Processes in a System of Two Spins, Physical Review, 99 (1955) 559–565.

[22]. Dhimitruka I, Grigorieva O, Zweier JL, Khramtsov VV, Synthesis, structure, and EPR characterization of deuterated derivatives of Finland trityl radical, Bioorg Med Chem Lett, 20 (2010) 3946–3949. [PubMed: 20537895]

[23]. Ardenkjaer-Larsen JH, Laursen I, Leunbach I, Ehnholm G, Wistrand LG, Petersson JS, Golman K, EPR and DNP properties of certain novel single electron contrast agents intended for oximetric imaging, J Magn Reson, 133 (1998) 1–12. [PubMed: 9654463]

[24]. Krynicki K, Proton spin-lattice relaxation in pure water between 0°C and 100°C, Physica, 32 (1966) 167–178.

[25]. Armstrong BD, Han S, A new model for Overhauser enhanced nuclear magnetic resonance using nitroxide radicals, J Chem Phys, 127 (2007) 104508. [PubMed: 17867762]

[26]. Matsumoto S, Utsumi H, Aravalluvan T, Matsumoto K, Matsumoto A, Devasahayam N, Sowers AL, Mitchell JB, Subramanian S, Krishna MC, Influence of proton T1 on oxymetry using Overhauser enhanced magnetic resonance imaging, Magn Reson Med, 54 (2005) 213–217. [PubMed: 15968662]

[27]. Christmas KM, Bassingthwaighte JB, Equations for O2 and CO2 solubilities in saline and plasma: combining temperature and density dependences, J Appl Physiol (1985), 122 (2017) 1313–1320. [PubMed: 28235861]

[28]. Teng CL, Hong H, Kiihne S, Bryant RG, Molecular oxygen spin-lattice relaxation in solutions measured by proton magnetic relaxation dispersion, J Magn Reson, 148 (2001) 31–34. [PubMed: 11133273]

[29]. Laurent S, Elst LV, Muller RN, Comparative study of the physicochemical properties of six clinical low molecular weight gadolinium contrast agents, Contrast Media Mol Imaging, 1 (2006) 128–137. [PubMed: 17193689]

[30]. Wang Y, Spiller M, Caravan P, Evidence for weak protein binding of commercial extracellular gadolinium contrast agents, Magn Reson Med, 63 (2010) 609–616. [PubMed: 20146229]

[31]. Vallet P, Van Haverbeke Y, Bonnet PA, Subra G, Chapat JP, Muller RN, Relaxivity enhancement of low molecular weight nitroxide stable free radicals: importance of structure and medium, Magn Reson Med, 32 (1994) 11–15. [PubMed: 8084224]

[32]. Bobko AA, Eubank TD, Driesschaert B, Dhimitruka I, Evans J, Mohammad R, Tchekneva EE, Dikov MM, Khramtsov VV, Interstitial Inorganic Phosphate as a Tumor Microenvironment Marker for Tumor Progression, Scientific Reports, 7 (2017) 41233. [PubMed: 28117423]

[33]. Persson BRR, Lars M, Leif GS, Paramagnetic Ions Affect Relaxation Rate Dispersion of Blood: Implications for Magnetic Resonance Relaxation Dispersion Imaging, Journal of Bioengineering & Biomedical Science - 2 (2011) - 1–8.

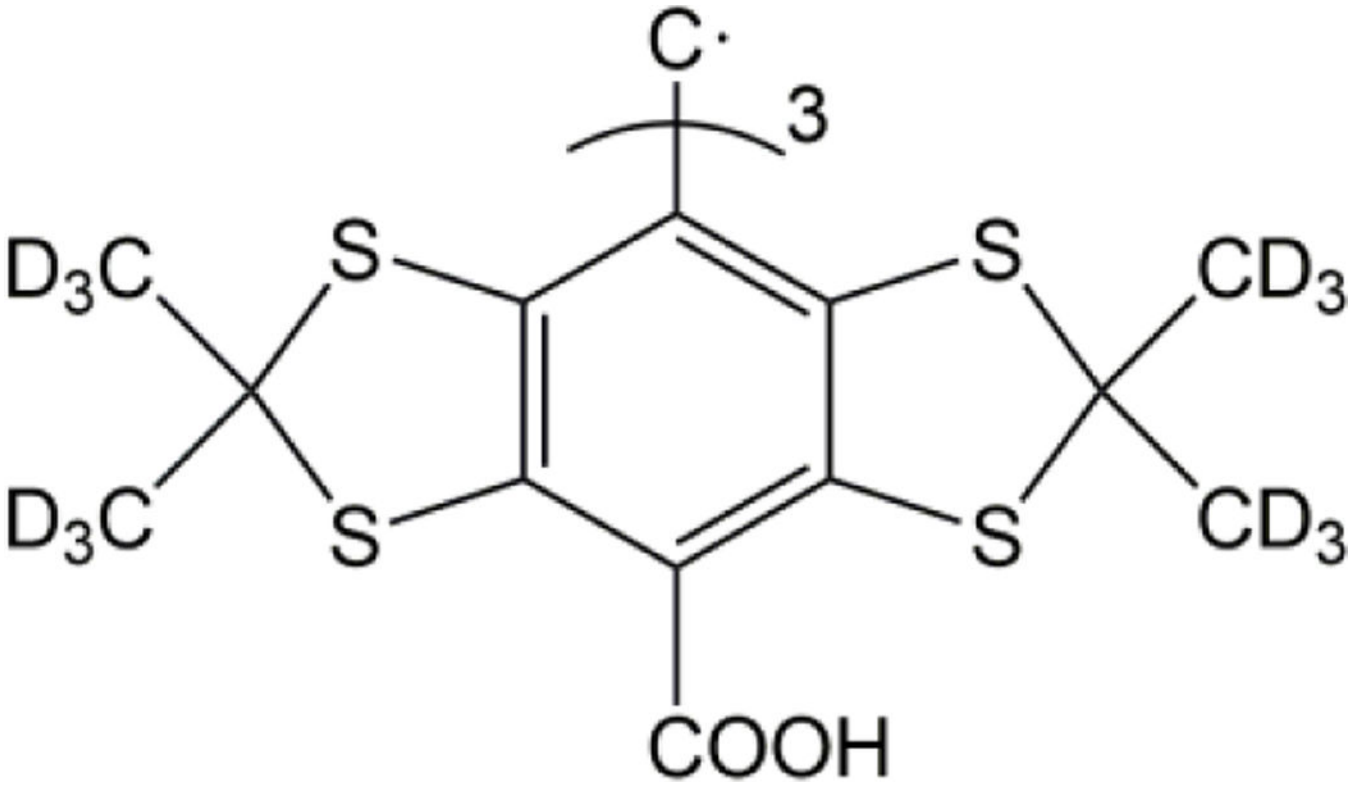

Fig. 1.
Structure of deuterated “Finland” trityl radical.

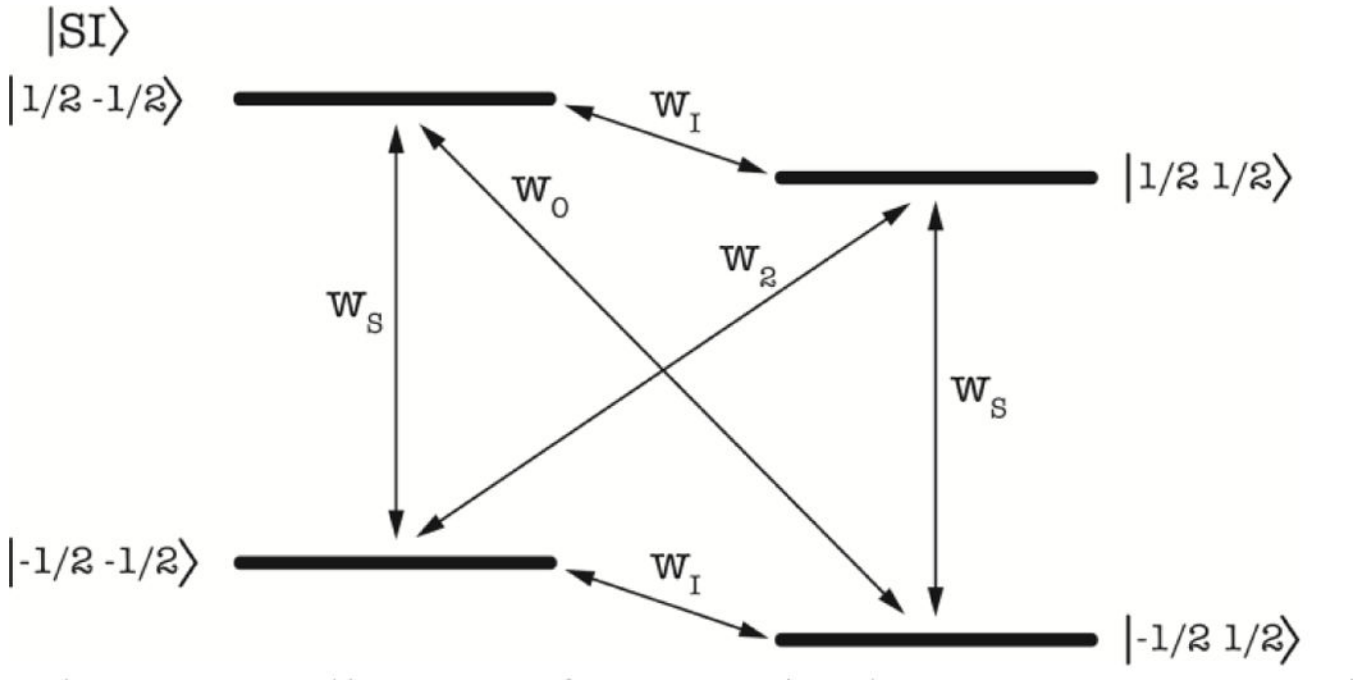

Fig. 2.

Spin states diagram for unpaired contrast agent electron spin and solvent proton spin. The rates of the transitions are denoted by the corresponding symbols shown over the arrows: w_1 - nuclear transition, w_s - electron transition and w_0 and w_2 - zero and double quantum transitions induced by dipole-dipole and contact interactions.

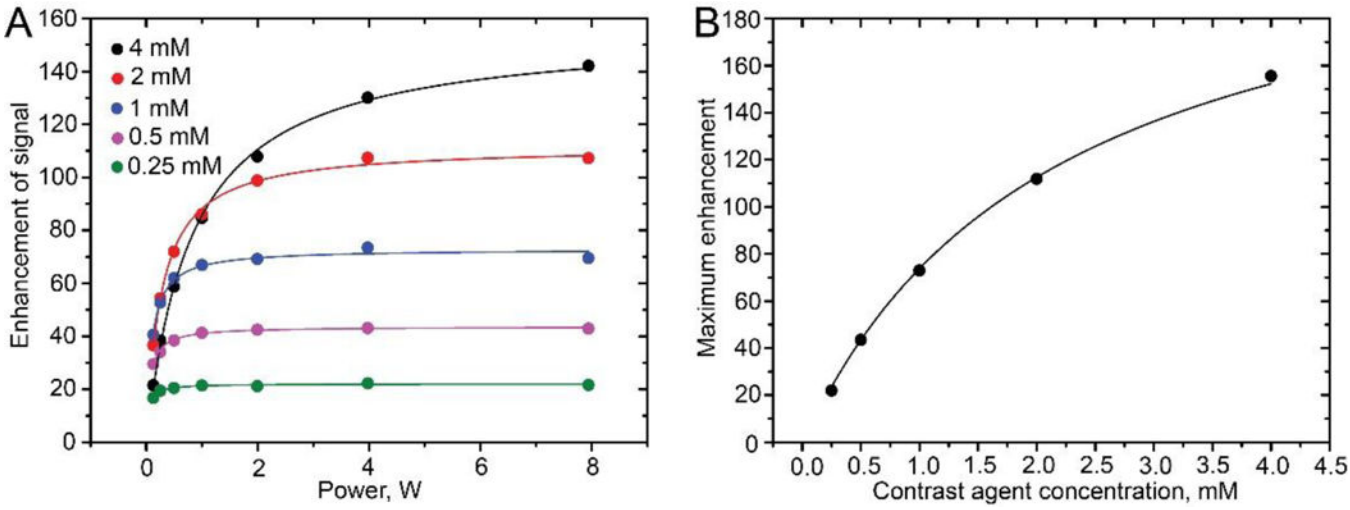

Fig. 3.

(**A**) Dependence of enhancement on irradiation power measured at different contrast agent concentrations in anaerobic conditions; solid lines are the best fits of equation (12) to the experimental data yielding the values of maximum enhancement. (**B**) Dependence of maximum enhancement on contrast agent concentration; solid line is the best fit of equation (6) to the E_{max} data yielding the value of coupling factor, **ε**, equal to 0.357±0.003 and enhancement at infinite power and contrast agent concentration, E_{max}^{inf}, equal to 236±2.

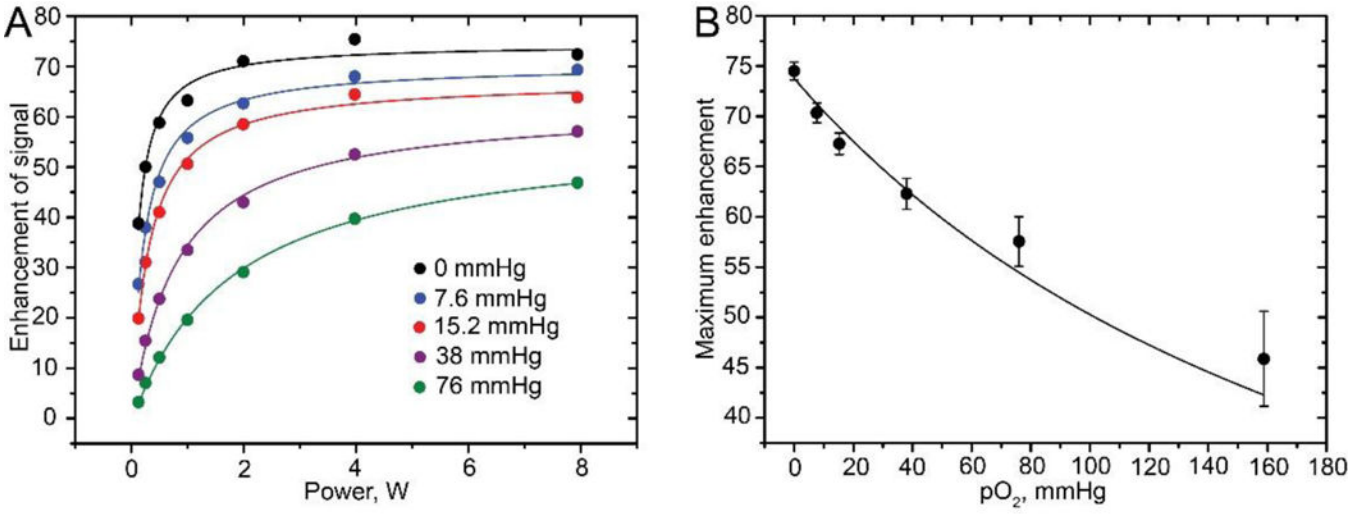

Fig. 4.

(**A**) Dependence of enhancement on irradiation power for contrast agent concentration 1 mM and different pO_2; fitting equation (8) to the experimental data yields contrast agent and pO_2 listed in Table 1. (**B**) Dependence of the maximum enhancement on pO_2; fitting equation (9) to the E_{max} data yields the value of leakage rate constant w_l^0 equal to $(1.7\pm0.2)\times10^{-3}$ $(mmHg\cdot s)^{-1}$.

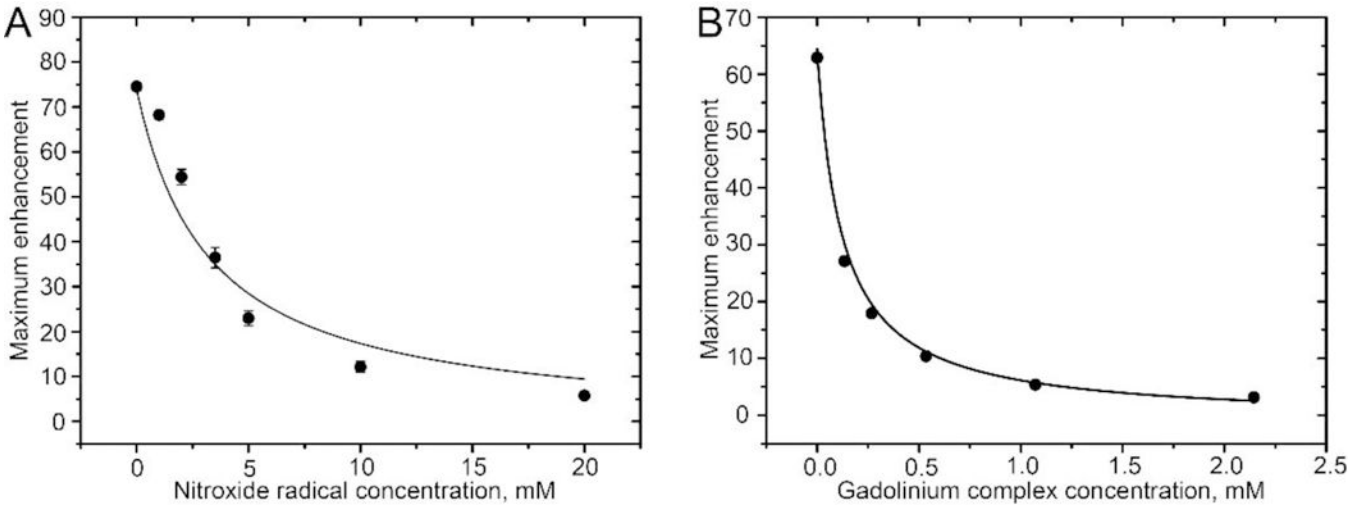

Fig. 5.

(**A**) Dependence of maximum enhancement on nitroxide radical concentration measured at trityl contrast agent concentration of 1 mM. Fitting equation (9) to the E_{max} data yields the value of leakage rate constant w_l^0 equal to 0.11±0.02 $(mM{\cdot}s)^{-1}$;.(**B**) Dependence of the maximum enhancement on gadolinium complex concentration measured at trityl contrast agent concentration of 0.83 mM. Fitting equation (9) to the E_{max} data yields the value of w_l^0, equal to 5.0±0.3 $(mM{\cdot}s)^{-1}$.

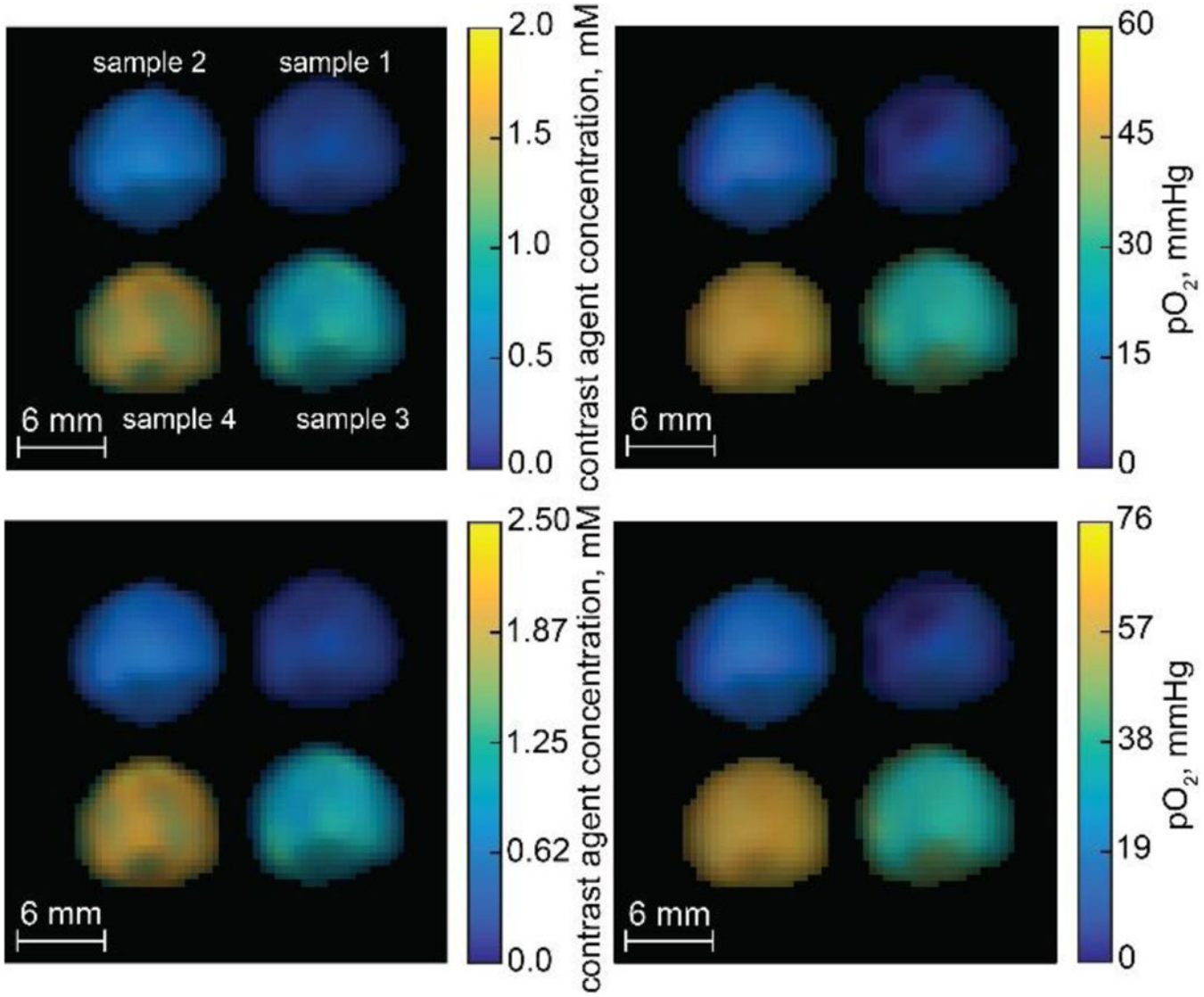

Fig. 6.

2D maps of contrast agent and pO_2 distribution in phantom samples. Phantom consisted of four tubes with spin probe concentrations 0.25, 0.5, 1 and 2 mM and pO_2 values 0, 15.2, 38 and 76 mmHg for the tube samples 1, 2, 3, and 4, correspondingly. Top: calculation with leakage factor f Bottom: calculation with leakage factor f^* Resonator efficiency factor α = 5.7 $\mu T^2/W$. Acquisition parameters are: T_{EPR}, 500 ms; T_R, 700 ms; T_E, 37 ms; matrix, 64×64; field of view, 30×30 mm^2; slice thickness, 100 mm; total acquisition time, 3 min; EPR frequency 451.9 MHz; applied powers of EPR irradiation, 0.5 and 8 W; NMR frequency, 686.3 kHz.

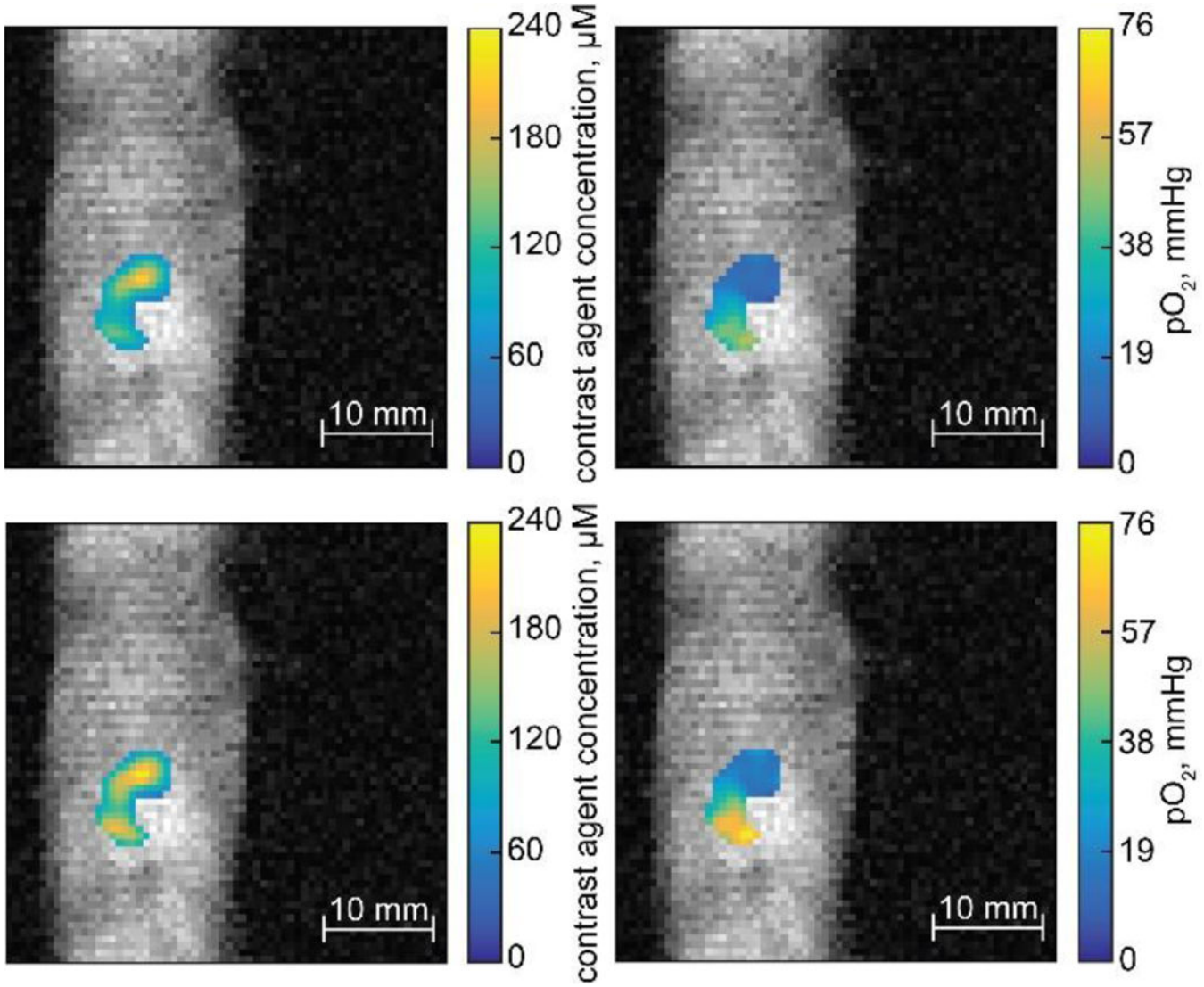

Fig. 7.

2D maps of contrast agent and oxygen partial pressures in mouse tumor superimposed with the MRI image. Top: calculation with leakage factor *f*. Bottom: calculation with leakage factor *f** Resonator efficiency factor, = 3.5 $\mu T^2/W$. Acquisition parameters were as follows: T_{EPR}, 500 ms; T_R, 700 ms; T_E, 37 ms; matrix, 64×64; field of view, 40×40 mm^2; slice thickness, 5 mm; total acquisition time, 3 min; EPR frequency 451.9 MHz; applied powers of EPR irradiation, 1 and 8 W; NMR frequency, 686.3 kHz.

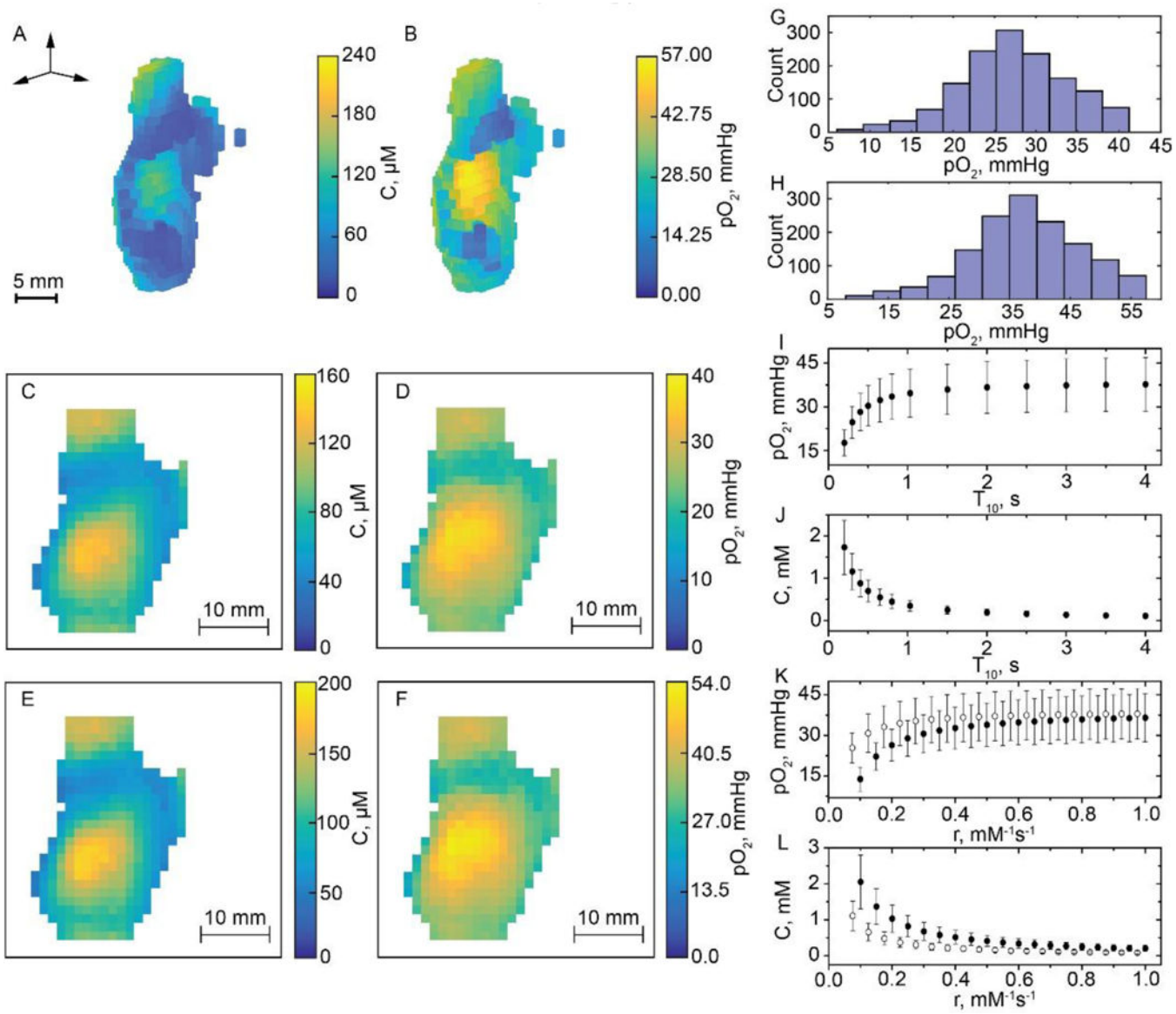

Fig. 8.

3D maps of contrast agent (A) and oxygen partial pressures (B) in mouse tumor. Parameters were calculated using system of equations with leakage factor *f** Resonator efficiency factor, $\alpha = 2\ \mu T^2/W$. Acquisition parameters were as follows:, T_{EPR} 500 ms; T_R, 1200 ms; T_E, 37 ms; matrix, 32×32; field of view, 40×40 mm^2; total acquisition time, 16 min; EPR frequency 451.9 MHz; applied powers of EPR irradiation, 1 and 16 W; NMR frequency,686.3 kHz. 2D coronal projection (C, D, E, F) of 3D maps of contrast agent and oxygen partial pressures in mouse tumor. C and D: calculation with leakage factor *f* E and F: calculation with leakage factor *f** Histograms of pO_2 distribution in mouse tumor. (**G**) Calculation with leakage factor *f* (**H**) Calculation with leakage factor *f** The obtained mean values and standard deviations: 27±7 mmHg and 38±9 mmHg for calculations performed with factors *f* and *f**, correspondingly. Dependences of mean pO_2 (I) and spin probe concentration (J) values on relaxation time T_{10} at spin probe relaxivity r=0.12 $mM^{-1}s^{-1}$. Error bars represent the

standard deviation values. Dependences of mean pO_2 (K) and spin probe concentration (L) values on spin probe relaxivity (r) at relaxation time T_{10}=0.2 (filled circles) and 0.5 (empty circles) s. Error bars represent the standard deviation values.

Table 1

Prepared and calculated contrast agent (C) and oxygen partial pressures (pO_2) and their standard errors. Calculations were done using mean data from OMRI images obtained at powers: 0.125; 0.25; 0.5; 1.0; 2.0; 4.0 and 8.0 W

Sample №	Prepared		Calculation with leakage factor *f*		Calculation with leakage factor f^*	
	C, mM	pO_2, mmHg	C, мМ	pO_2, mmHg	C, mM	pO_2, mmHg
1	1	0	0.97±0.02	0.6±0.8	1.01±0.03	0±1
2	1	7.6	0.90±0.02	7.6±0.8	0.98±0.02	9±1
3	1	15.2	0.84±0.02	12±1	0.96±0.02	15±1
4	1	38	0.76±0.02	31±1	0.99±0.03	41±2
5	1	76	0.68±0.02	56±2	1.04±0.03	75±2

Table 2

Prepared and calculated contrast agent (C) and oxygen partial pressures (pO_2) and their standard deviations. Calculations were done using two OMRI images obtained at irradiation powers 0.5 and 8.0 W

Sample №	Prepared		Calculation with leakage factor *f*		Calculation with leakage factor f^*	
	C, mM	pO_2, mmHg	C, mM	pO_2, mmHg	C, mM	pO_2, mmHg
1	0.25	0	0.23±0.03	5±3	0.25± 0.03	6±3
2	0.5	15.2	0.40±0.06	10±3	0.44± 0.06	13±4
3	1	38	0.80±0.12	30±3	1.0±0.15	39±4
4	2	76	1.40±0.15	52±3	2.0±0.2	66±4